Dispersion in dielectric-lined waveguides designed for terahertz-driven deflection of electron beams

V. Georgiadis,[1,2,a)] A. L. Healy,[1,3,a)] M. T. Hibberd,[1,2] G. Burt,[1,3] S. P. Jamison,[1,4] and D. M. Graham[1,2,b)]

[1)] *The Cockcroft Institute, Sci-Tech Daresbury, Keckwick Lane, Daresbury, Warrington WA4 4AD, UK*

[2)] *Department of Physics and Astronomy & Photon Science Institute, The University of Manchester, Oxford Road, Manchester M13 9PL, UK*

[3)] *Department of Engineering, Lancaster University, Bailrigg, Lancaster LA1 4YW, UK*

[4)] *Department of Physics, Lancaster University, Bailrigg, Lancaster LA1 4YW, UK*

(Dated: 18 February 2021)

We have developed dielectric-lined rectangular waveguide structures for terahertz (THz)-driven ultrafast deflection of 100 keV electron beams. The structures were designed to achieve THz phase velocity matching with co-propagating electron bunches. The phase-matching capability was experimentally confirmed through time-frequency analysis of the broadband coherent THz transmission measured by electro-optic sampling. The analysis determined both the frequency dependent propagation constants in the electron interaction region, and the propagation characteristics of the integrated THz tapered coupler.

[a)] These two authors contributed equally

[b)] Electronic mail: Darren.Graham@manchester.ac.uk

Dielectric terahertz (THz) waveguides are of significant interest due to their capability for low transmission loss, and low group- and phase-velocity dispersion, facilitating the undistorted propagation of sub-picosecond THz pulses[1]. Rectangular metal THz waveguides have also been shown to provide large sensitivity enhancements in the spectroscopic measurement of *in-situ* dielectrics (thin film or gas).[2] In addition, dielectric-lined cylindrical[3,4] and rectangular[5] waveguides have been employed together with relativistic electron beams for bunch-driven generation of coherent narrow-band THz radiation. A relatively new application area of dielectric-lined waveguides (DLWs) has been in the field of THz-driven electron acceleration and manipulation, where their use together with intense ultrafast THz pulses is facilitating the development of compact particle accelerators[6,7] and the metrology of ultrashort electron beams[8].

One of the key challenges in the field of THz-driven electron acceleration and electron beam manipulation is increasing the THz-electron interaction length. This can in principle be achieved by matching the phase- and group-velocity of the THz pulse to the sub-luminal velocity of the electron bunch. However in matching the phase velocity to achieve monotonic acceleration or deflection, a pulse group velocity mismatch is introduced. The group velocity mismatch limits the interaction length by pulse slippage. One solution recently proposed is to utilize an optical pulse front tilt to generate a travelling THz source along the exit surface of a lithium niobate ($LiNbO_3$) crystal, enabling sub-luminal propagation of a THz pulse at a phase velocity determined by the tilt angle.[9] An inverse FEL interaction scheme has also been presented,[10] although such a scheme is intrinsically self-limiting and not able to offer continuing acceleration. A more widely explored approach has been in using dielectric-lined metallic waveguide structures. Demonstrations have included acceleration of non-relativistic electrons using high-field strength THz radiation in a cylindrical DLW[6], and phase-velocity matched acceleration of relativistic electrons in a rectangular DLW[7]. A segmented THz device, consisting of multiple dielectric loaded metallic waveguides transverse to the electron motion has also recently been demonstrated to provide electron acceleration or streaking, depending on the mode of operation.[8] The THz-particle interaction of the segmented device was fixed by the number of waveguides and their transverse dimension to a length of less than 1 mm, although this could in principle be increased by adding more waveguide layers, provided more THz energy was available to accommodate the extra segments. In contrast, the phase- and group-velocity dispersion in the DLWs employed by

Nanni *et al.*[6] and Hibberd *et al.*[7] limited the interaction length to 3 mm and 4 mm, respectively, a small fraction of the physical length of the waveguides employed. To reach the ultimate group-velocity walk-off interaction limit of the DLWs requires THz pulses with a bandwidth optimized to minimize the effects of dispersion. To calculate the optimum bandwidth required and thereby maximise the interaction requires knowledge of DLW dispersion. The dispersion limited interaction lengths therefore highlight the need for characterizing the DLW dispersion properties in order to develop effective THz-driven particle accelerators and manipulation devices.

Terahertz time-domain spectroscopy and imaging has been used to measure both single-mode and mode-specific dispersion in cylindrical dielectric and dielectric-lined waveguides[11–13]. A standard method utilized to determine the mode dispersion in uniform cross-section waveguides is the so-called cut-back technique[1,14–16], whereby sub-picosecond THz pulses propagating through two different lengths of waveguide are compared. The reduction in length (or cut back) occurs from the output end of the waveguide, so that the input coupling remains identical and therefore eliminates the need to determine the input coupling efficiency.

In this letter, we describe a DLW that was designed for the deflection of electron bunches with an energy of 100 keV, corresponding to an electron velocity of $0.548c$. The structure was designed to deflect electrons using both broadband single-cycle and narrow-band multi-cycle THz pulses with a center frequency of approximately 0.5 THz. We use the cut-back technique with THz electro-optic sampling to experimentally characterize the dispersion of a waveguide structure with an input coupling horn. We establish the dispersion relation of individual components of the DLW structure, the waveguide and coupler. The dispersion measurements were verified by electromagnetic field simulations, and the results applied to determine the performance of the structure as a THz-driven electron deflector.

The dimensions of the waveguide were selected to match the phase-velocity of the deflecting Longitudinal Section Magnetic LSM_{01} waveguide mode to the electron velocity.[17] While a waveguide design which matches both the phase- and group-velocity is technically possible for a deflecting mode, it was determined that for a typical THz input pulse the maximum integrated deflection was obtained with a design that had a group-velocity less than the phase-velocity. The LSM_{01} mode inside the waveguide has a variable transverse field component across the vacuum aperture (as shown by the electric field in the vector plot

inset of Fig. 1), with a non-zero deflecting field at the centre. There is also a longitudinal electric field component associated with the LSM_{01} mode, but it has a $\pi/2$ phase offset and therefore zero amplitude at the centre of the aperture when the transverse component is maximum.

The waveguide comprised of a 1 mm wide hollow rectangular copper structure lined at the top and bottom with 240 μm-thick fused quartz (Infrasil 302), with a 200 μm-thick free space aperture in the center for electron beam propagation. The fused quartz was purchased in sheets of thickness 240$\pm$10 μm, with a reported thickness variation across the sheet of $\pm$1 μm, cut into the required sizes and secured to the waveguide walls with glycol phthalate (Crystalbond adhesive). The structure was manufactured in two parts, with the top and bottom sections joined together with the aid of alignment pins. A linearly tapered horn coupler (without a dielectric lining) with an entrance aperture height of 5 mm, width of 10 mm, and length of 44 mm was incorporated in the design to efficiently couple free-space Gaussian-profiled THz pulses with linear polarization into the desired LSM_{01} waveguide mode, and thereby suppress coupling to higher modes. This reduces reflections due to mismatch at the DLW entrance, but introduces further dispersive effects as the coupler is itself a metallic waveguide. In order to enable the determination of the dispersion of the DLW and remove the influence of the coupler, two nominally identical structures were manufactured with DLW lengths of 5 mm and 10 mm (total structure lengths of 49 mm and 54 mm with the input coupler).

Measurements of the THz transmission through the DLW structure (waveguide plus coupler) were performed using a custom-built THz time-domain spectrometer employing a 1 kHz regenerative amplifier laser system, which produced 100 fs pulses with a central wavelength of 800 nm and a maximum pulse energy of 500 μJ. A schematic diagram of the experimental setup is shown in Fig. 1. The pump beam was expanded to a beam diameter of 20 mm ($1/e^2$) and directed onto a spintronic THz emitter that was placed between two neodymium disc magnets. The applied magnetic field pattern dictated the polarization state of the THz radiation emitted[18]. In this work the magnets were orientated with an aligned polarity to generate a linearly polarized THz beam in order to excite the LSM_{01} mode in the DLW.

The emitter (a bilayer structure of $Co_{20}Fe_{60}B_{20}$/Pt thin films deposited on a 500 μm-thick fused silica substrate by DC magnetron sputtering) was excited at normal incidence from the substrate side and a filter was used to block the residual 800 nm radiation transmitted

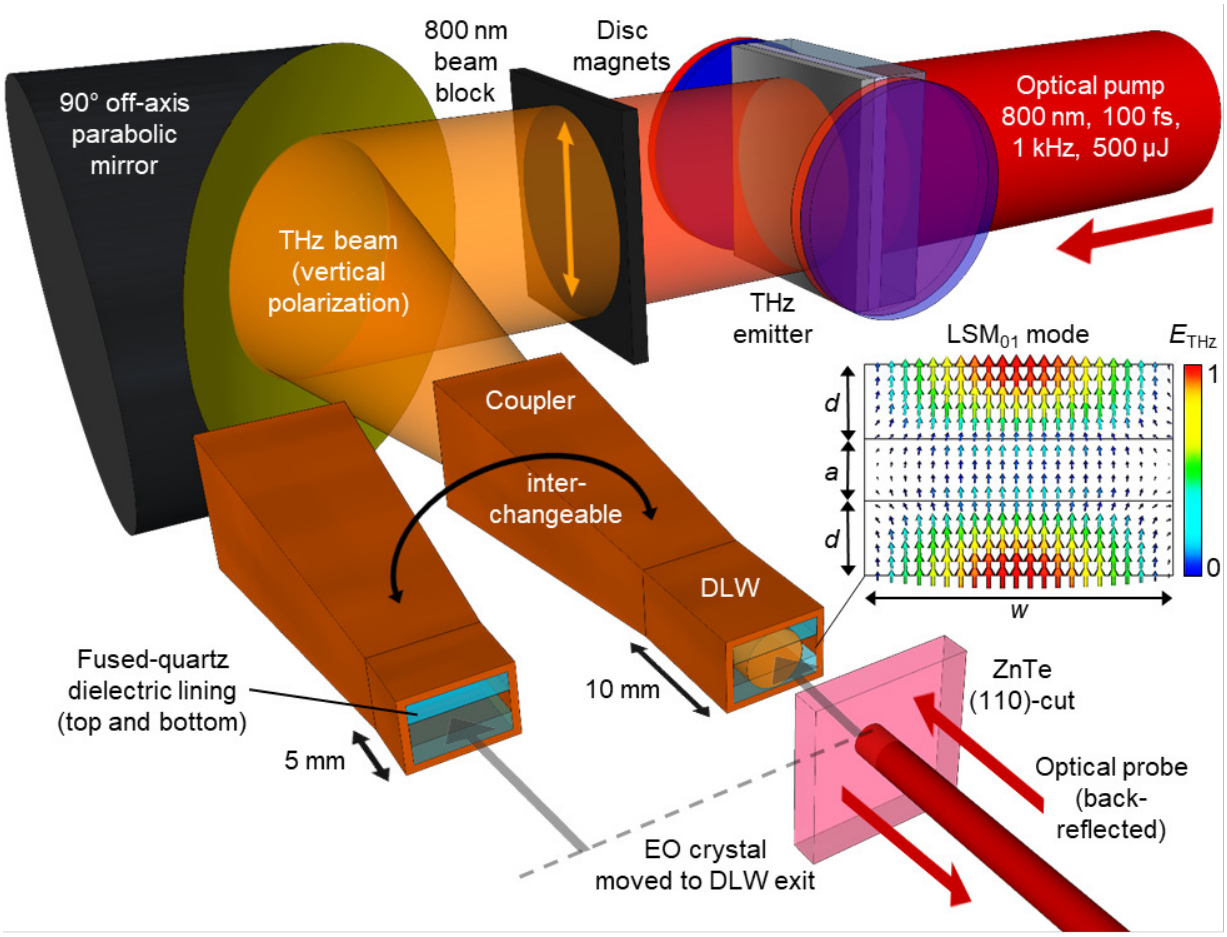

FIG. 1. Schematic diagram of the experimental setup showing the generation of vertically polarized THz radiation, and its coupling into the dielectric-lined waveguide structure. The transmitted THz radiation was detected using an electro-optic crystal in a back-reflection geometry. Inset shows the simulated LSM_{01} mode profile inside the waveguide where a is the waveguide free space aperture, d is the dielectric thickness, and w is the width of the waveguide.

through the emitter. The generated THz radiation was focused by a 50.8 mm-diameter gold 90° off-axis parabolic mirror with a focal length of 101.6 mm into the center of the waveguide coupler. The THz radiation transmitted through the DLW structure was measured using a 2 mm-thick (110)-cut ZnTe crystal placed at the exit of the DLW and utilized a back-reflected 100 μm diameter probe beam in a standard electro-optic sampling scheme to detect the transmitted vertically polarized electric field. All the measurements were performed at room temperature and at a relative humidity of 5-6% to reduce the absorption of the THz

radiation by water vapor.

Figures 2(a) and (b) show the THz waveforms measured before and after transmission through the DLW structures. The spintronic emitter produced a single-cycle THz pulse with a duration of 1.9 ps ($1/e^2$ of the field envelope), which was stretched to approximately 16.8 ps and 29.0 ps after propagation through the structures which incorporated the 5 mm and 10 mm long waveguides, respectively. The spintronic emitter produced a second THz emission pulse at approximately 6.7 ps after the main pulse, which was attributed to the reflection of the 800 nm pump pulse inside the fused silica substrate of the emitter. This reflection results in Fourier transform oscillation artefacts observed in the amplitude spectrum shown in Fig. 2(d). The reflection also distorts the THz waveforms measured after transmission through the DLW structures, shown in Figs. 2(a) and (b), as the main transmitted pulse is broadened such that it overlaps with the reflection in time. To remove the reflection from the analysis we consider a measured field $S(t)$ as a combination of initial spintronic emission $E(t)$ and a reflected pulse as

$$S(t) = E(t) + rE(t - \tau),$$

where the reflection is characterized by a shift in the time delay of the initial peak, τ, and a reduction in amplitude by a factor of r. The Fourier transform results in

$$E(\omega) = S(\omega)/(1 + r \exp[-i\omega\tau]),$$

and through an inverse Fourier transform provides, $E(t)$, which is free from the reflection artefact, as discussed by Naftaly and Miles.[19] The values of r and τ were measured from the reference waveform and then applied to the waveforms transmitted through the DLW structures in order to remove the influence of the reflection, as shown by the corrected waveforms in Figs. 2(a) and (b).

Figures 2(d) and (f) show the amplitude spectra of reference and waveguide transmitted THz pulses. The spectra in Fig. 2(f) show a sharp drop in amplitude at 0.12 ± 0.01 THz and 0.10 ± 0.01 THz for the DLW structure incorporating the 10 mm and 5 mm waveguide, respectively. This is in good agreement with the waveguide cut-off frequency of 0.1 THz, calculated from electromagnetic field simulations using CST Studio Suite[20]. The dispersion relation was calculated using the Eigenmode Solver in CST Studio Suite together with the dimensions of the DLW structure and a relative permittivity of 3.81 for the fused-quartz dielectric lining[21].

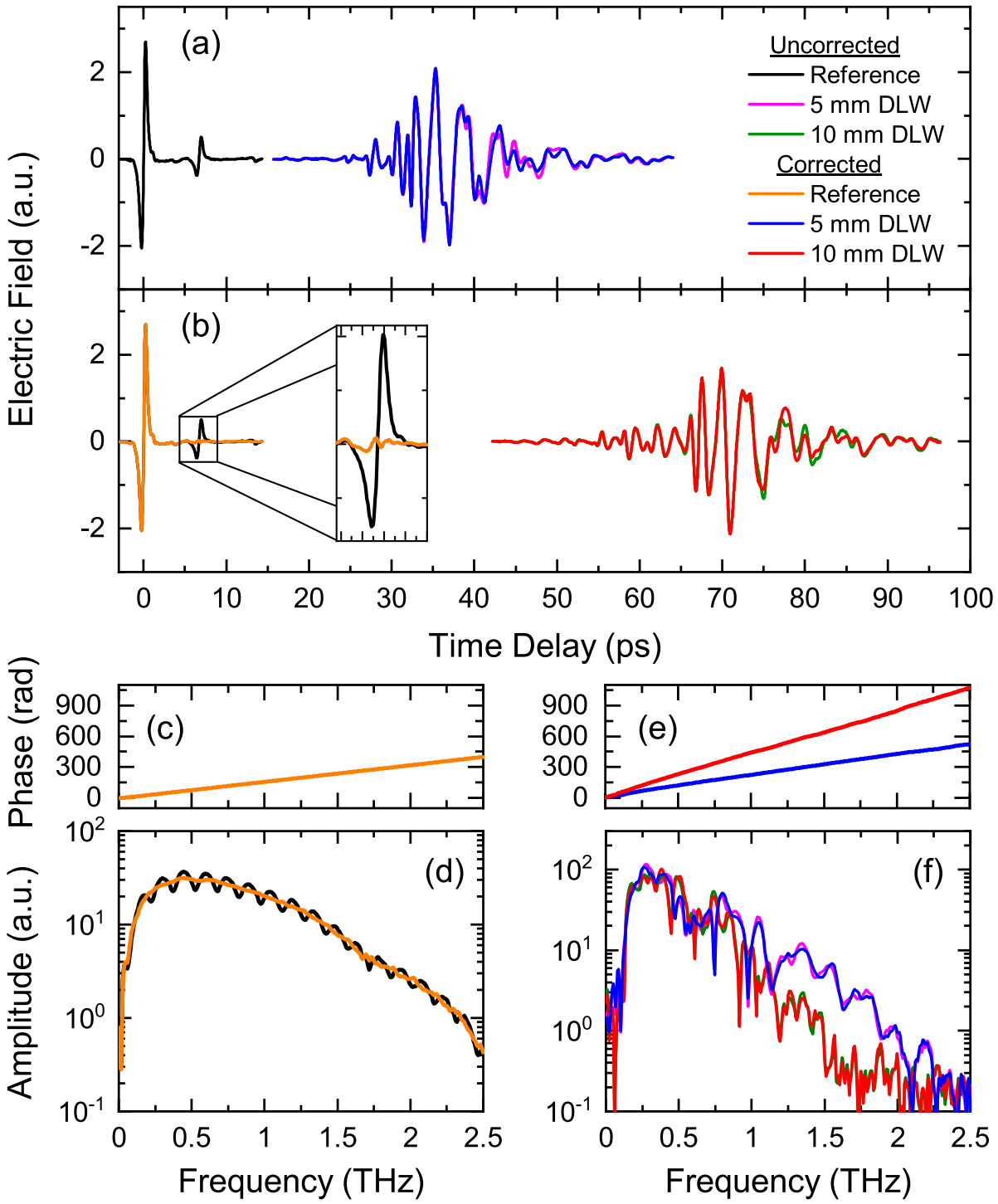

FIG. 2. Terahertz waveforms transmitted through (a) the 5 mm long dielectric-lined waveguide (DLW) structure, (b) the 10 mm long DLW structure, together with an air reference with and without a reflection pulse removal correction applied (see text for details). Inset shows the effect of the reflection removal correction on a second THz pulse emitted from the source due to the pump pulse reflection. The corresponding phase and amplitude spectra for the air reference, (c) and (d), and for the DLW structures, (e) and (f), respectively.

The reference and transmitted THz waveforms were used to obtain the dispersion of the DLW structures. The waveforms however include the dispersive effect of the coupler, in addition to that of the DLW. To calculate the dispersion of the DLW alone and separate out the influence of the coupler, two nominally identical structures were used, one which incorporated a waveguide with length $L_{\mathrm{long}} = 10\,\mathrm{mm}$ and one with length $L_{\mathrm{short}} = 5\,\mathrm{mm}$. The dispersion for a section of DLW of length $L_{\mathrm{long}} - L_{\mathrm{short}}$ can be expressed by the propagation constant, $\beta_{\mathrm{wg}}(\omega)$, which is related to the waveforms transmitted through the DLWs by

$$\beta_{\mathrm{wg}}(\omega) = \frac{1}{L_{\mathrm{long}} - L_{\mathrm{short}}} \arg\left[\frac{\widetilde{E}(\omega)_{\mathrm{long}}}{\widetilde{E}(\omega)_{\mathrm{short}}}\right],$$

where $\widetilde{E}(\omega)_{\mathrm{long}}$ and $\widetilde{E}(\omega)_{\mathrm{short}}$ are the complex electric field at angular frequency ω at the exit of the long and short length waveguide, respectively. Once the propagation constant of the waveguide was determined, an effective phase shift for the the coupler, $\beta_{\mathrm{c}}(\omega)$ was ascertained from a comparison of the reference and a waveform transmitted through one of the DLW structures $\widetilde{E}(\omega)_{\mathrm{wg}}$ by

$$\beta_{\mathrm{c}}(\omega) = \frac{\arg\left[\frac{\widetilde{E}(\omega)_{\mathrm{wg}}}{\widetilde{E}(\omega)_{\mathrm{ref}}}\right] - \beta_{\mathrm{wg}}(\omega)L_{\mathrm{wg}} + k(L_{\mathrm{c}} + L_{\mathrm{wg}})}{L_{\mathrm{c}}},$$

where $k(L_{\mathrm{c}} + L_{\mathrm{wg}})$ accounts for the fact that the reference waveform, $\widetilde{E}(\omega)_{\mathrm{ref}}$, propagated through air a distance of $L_{\mathrm{c}} + L_{\mathrm{wg}}$ to reach the detector.

The propagation constant $\beta_{\mathrm{wg}}(\omega)$ and the effective phase shift $\beta_{\mathrm{c}}(\omega)$ determined experimentally are shown in Fig. 3(a) together with the values calculated from electromagnetic field simulations. As can be seen, the simulations are in good agreement over the range of approximately 0.1-0.6 THz.

The corresponding phase and group velocity for the DLW are given in Fig. 3(b). At the design frequency of 0.47 THz, the dispersion relation of the LSM_{01} mode results in mode propagation at a phase velocity, v_{p}, of $0.548 \pm 0.002c$ matching the $0.548c$ velocity of 100 keV electrons.

The group-velocity dispersion of the DLW structure is visualized with Wigner-Ville spectra[25,26] in Fig. 4 where the reference waveform in Fig. 4(a) reveals the expected zero group velocity dispersion with all frequency components of the broadband THz pulse temporally overlapped in free space. In contrast, Fig. 4(b) shows the group delay dispersive effect of the 10 mm long DLW structure with integrated 44 mm long coupling horn, with

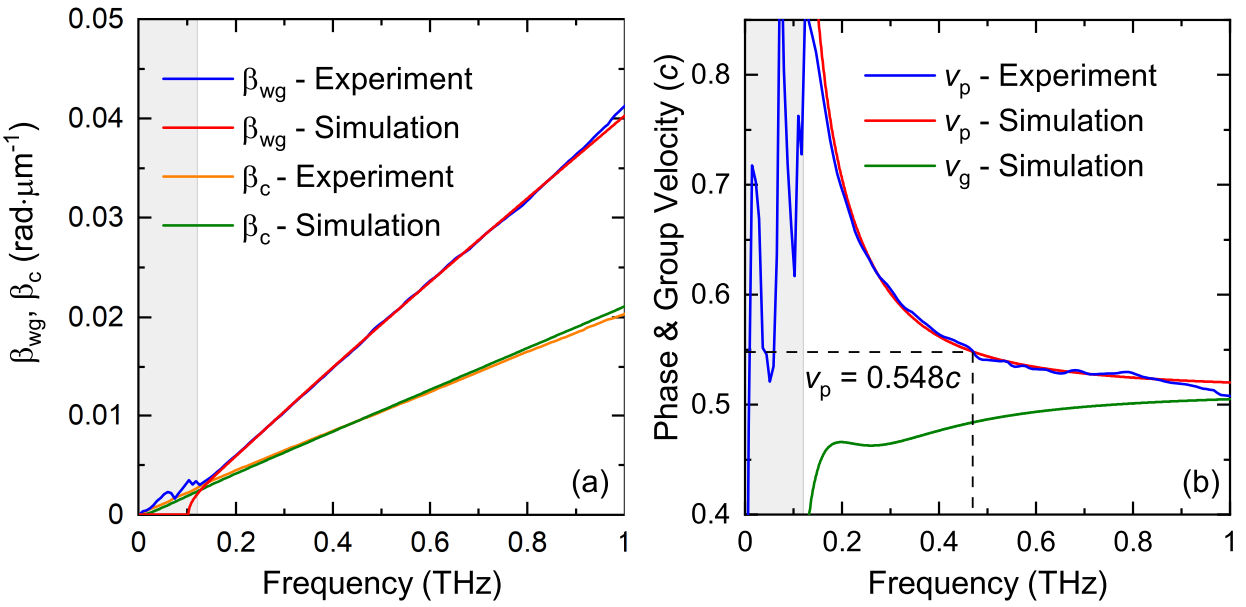

FIG. 3. (a) Propagation constant for the waveguide, β_{wg}, and the effective phase shift for the coupler, β_c, compared with the results of an electromagnetic field simulation (see text for details). (b) Phase velocity calculated from the waveguide propagation constant together with the phase and group velocities determined by simulation. Shaded areas indicate regions of uncertainty in the experimental data due to low spectral amplitude. The data has been corrected to remove small jumps in the THz phase from absorption by the well-known rotational transitions associated with residual water vapor.[24]

the higher frequency components arriving earlier in time, corresponding to negative chirp. The experimentally measured group-delay dispersion agrees well with a simulation of the propagation of a TE_{10} mode in the tapered coupler and a LSM_{01} mode in the DLW (see supplementary material for further details).

Having determined the dispersion in the DLW structure, it was possible to assess the potential of the structure as a THz-driven ultrafast electron deflector. Such THz-driven electron manipulation devices are currently being developed for the metrology of sub-picosecond electron bunches[22,23], where the deflection is used to map the temporal structure of a bunch to an angular distribution for visualization on a screen. An ideal device would produce a large deflection rate or streaking speed in order to enable the measurement of the short duration electron bunches with high temporal resolution.

The measured dispersion was used to calculate the streaking speed for an on-axis elec-

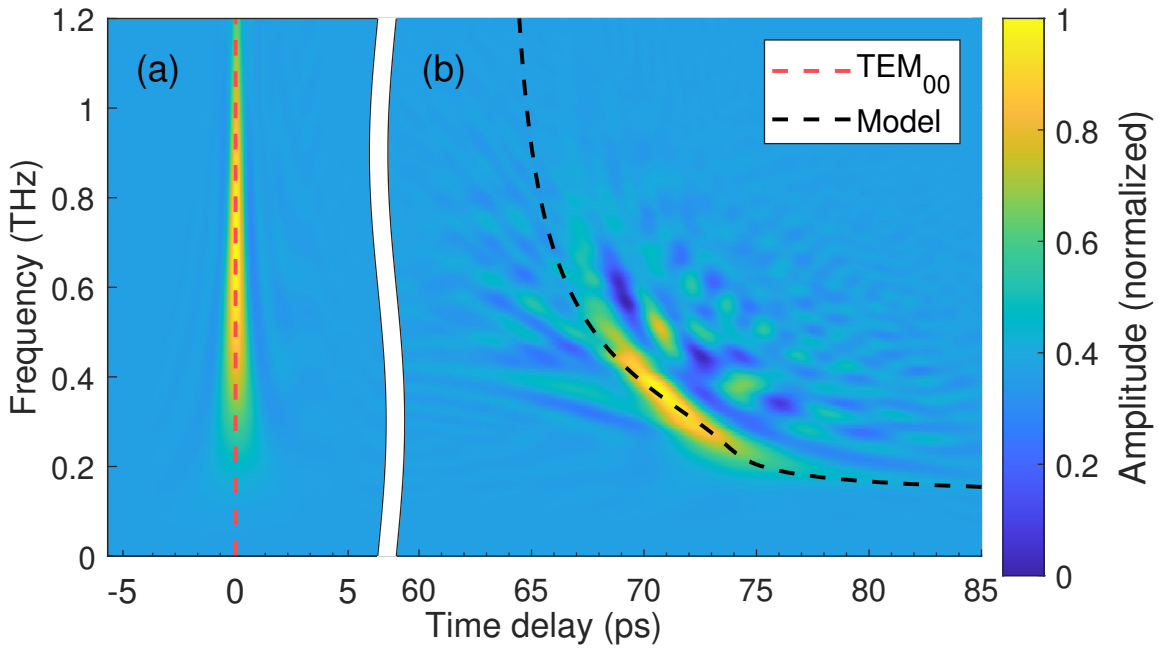

FIG. 4. Wigner-Ville spectra calculated from the THz waveform transmitted through (a) air and (b) the 10 mm long DLW structure. The reflection removal correction was applied to both waveforms. The black dashed line is the result of using an electromagnetic field simulation to determine the group-velocity dispersion in the DLW structure (the propagation of a TE_{10} mode in the tapered coupler and a LSM_{01} mode in the dielectric-lined waveguide).

tron beam travelling at $0.548c$ by integrating the transverse voltage applied on an electron[27] over a distance of 5 mm through the DLW (see supplementary material for details of the calculations). A streaking speed of approximately $330\,\mu\text{rad}\,\text{fs}^{-1}$ was calculated for a LSM_{01} mode with a central frequency of 0.47 THz, a bandwidth of 70 GHz (FWHM of power spectral density) and an energy of $6\,\mu$J inside the waveguide. In comparison, experimental measurements of the segmented waveguide device reported by Zhang *et al.*[8] revealed a maximum deflection rate or streaking speed of $140\,\mu\text{rad}\,\text{fs}^{-1}$ for 55 keV electrons, while metallic slits have been reported to provide maximum streaking speeds of $7.4\,\mu\text{rad}\,\text{fs}^{-1}$ using single-cycle THz pulses[22,23]. The streaking speed scales as the square-root of the input pulse energy. The DLW structure reported here therefore produces a normalized streaking speed of $135\,\mu\text{rad}\,\text{fs}^{-1}\,\mu\text{J}^{-1/2}$ when the deflecting LSM_{01} mode has a bandwidth of 70 GHz, only reducing to $82\,\mu\text{rad}\,\text{fs}^{-1}\,\mu\text{J}^{-1/2}$ when a broader bandwidth of 300 GHz (typical of a single-cycle THz pulse generated in a $LiNbO_3$ crystal) is considered. It should be noted however that

this calculation only considers electrons propagating through the structure on the central axis, and does not consider the THz input coupling efficiency. Nevertheless, the approach allows us to determine an upper limit to the streaking speed that may be obtained from a LSM_{01} deflecting mode for a given energy.

In summary, we have developed dielectric-lined rectangular waveguide structures for THz-driven ultrafast deflection of 100 keV electron beams. From a time-frequency analysis of broadband coherent THz transmission using electro-optic sampling, we determined the propagation constants for both the dielectric-lined waveguide structure and the integrated input coupling horn, confirming the THz phase velocity was matched to the $0.548c$ velocity of 100 keV electron beams. The frequency-dependent propagation constants measured were validated with electromagnetic field simulations, and the results used to determine that a DLW structure can provide a normalized streaking speed of $135\,\mu\mathrm{rad\,fs^{-1}}\,\mu\mathrm{J}^{-1/2}$.

See supplementary material for details of the streaking speed calculations, the deflecting bandwidth calculations, and the results of an electromagnetic field simulation showing the individual contribution of the coupler and the waveguide to the overall group-velocity dispersion.

We wish to acknowledge Rutherford Appleton Laboratory (RAL)-Space for the manufacture of the dielectric-lined waveguide structures. This work was supported by the United Kingdom Science and Technology Facilities Council [Grant Nos. ST/N00308X/1, ST/N003063/1 and ST/P002056/1]; and the Accelerator Science and Technology Centre through Agreement No. CN7214-SA98. The data associated with the paper are openly available from the Zenodo Data Repository at: http://dx.doi.org/xx.xxxxx/xxxxxx.x.

REFERENCES

[1]S. Atakaramians, S. Afshar V., T. M. Monro, and D. Abbott, Adv. Opt. Photonics **5**, 169 (2013).

[2]G. Gallot, S. P. Jamison, R. W. McGowan, and D. Grischkowsky, J. Opt. Soc. Am. B **17**, 851 (2000).

[3]G. Andonian, O. Williams, X. Wei, P. Niknejadi, E. Hemsing, J. B. Rosenzweig, P. Muggli,

M. Babzien, M. Fedurin, K. Kusche, R. Malone, and V. Yakimenko, Appl. Phys. Lett. **98**, 202901 (2011).

[4]S. Antipov, S. V. Baryshev, R. Kostin, S. Baturin, J. Qiu, C. Jing, C. Swinson, M. Fedurin, and D. Wang, Appl. Phys. Lett. **109**, 142901 (2016).

[5]T. H. Pacey, Y. Saveliev, A. Healy, P. G. Huggard, B. Alderman, P. Karataev, K. Fedorov, and G. Xia, Phys. Rev. Accel. Beams **22**, 091302 (2019).

[6]E. A. Nanni, W. R. Huang, K.-H. Hong, K. Ravi, A. Fallahi, G. Moriena, R. J. D. Miller, and F. X. Kärtner, Nat. Commun. **6**, 8486 (2015).

[7]M. T. Hibberd, A. L. Healy, D. S. Lake, V. Georgiadis, E. J. H. Smith, O. J. Finlay, T. H. Pacey, J. K. Jones, Y. Saveliev, D. A. Walsh, E. W. Snedden, R. B. Appleby, G. Burt, D. M. Graham, and S. P. Jamison, Nat. Photonics 14, 755 (2020).

[8]D. Zhang, A. Fallahi, M. Hemmer, X. Wu, M. Fakhari, Y. Hua, H. Cankaya, A.-L. Calendron, L. E. Zapata, N. H. Matlis, and F. X. Kärtner, Nat. Photonics **12**, 336 (2018).

[9]D. A. Walsh, D. S. Lake, E. W. Snedden, M. J. Cliffe, D. M. Graham, and S. P. Jamison, Nat. Commun. **8**, 421 (2017).

[10]E. Curry, S. Fabbri, J. Maxson, P. Musumeci, and A. Gover, Phys. Rev. Lett. **120**, 094801 (2018).

[11]O. Mitrofanov and J. A. Harrington, Opt. Express **18**, 1898 (2010).

[12]O. Mitrofanov, T. Tan, P. R. Mark, B. Bowden, and J. A. Harrington, Appl. Phys. Lett. **94**, 171104 (2009)

[13]S. P. Jamison, R. W. McGowan, and D. Grischkowsky, Appl. Phys. Lett. **76**, 1987 (2000).

[14]M. Nagel, A. Marchewka, and H. Kurz, Opt. Express **14**, 9944-9954 (2006).

[15]L.-J. Chen, H.-W. Chen, T.-F. Kao, J.-Y. Lu, and C.-K. Sun, Opt. Lett. **31**, 308-310 (2006).

[16]A. Dupuis, J.-F. Allard, D. Morris, K. Stoeffler, C. Dubois, and M. Skorobogatiy, Opt. Express **17**, 8012-8028 (2009).

[17]A. L. Healy, G. Burt, and S. P. Jamison, Nucl. Instrum. Methods Phys. Res. A **909**, 199 (2018).

[18]M. T. Hibberd, D. S. Lake, N. A. B. Johansson, T. Thomson, S. P. Jamison, and D. M. Graham, Appl. Phys. Lett. **114**, 031101 (2019).

[19]M. Naftaly, and R.E. Miles, Opt. Commun. **280**, 291-295 (2007).

[20]CST Studio Suite, 2020. http://www.cst.com.

[21]C. M. Randall and R. D. Rawcliffe, Appl. Opt. **6**, 1889-1895 (1967).

[22]R. K. Li, M. C. Hoffmann, E. A. Nanni, S. H. Glenzer, M. E. Kozina, A. M. Lindenberg, B. K. Ofori-Okai, A. H. Reid, X. Shen, S. P. Weathersby, J. Yang, M. Zajac, and X. J. Wang, Phys. Rev. Accel. Beams **22**, 012803 (2019).

[23]L. Zhao, Z. Wang, C. Lu, R. Wang, C. Hu, P. Wang, J. Qi, T. Jiang, S. Liu, Z. Ma, F. Qi, P. Zhu, Y. Cheng, Z. Shi, Y. Shi, W. Song, X. Zhu, J. Shi, Y. Wang, L. Yan, L. Zhu, D. Xiang, and J. Zhang, Phys. Rev. X **8**, 021061 (2018).

[24]H. M. Pickett, R. L. Poynter, E. A. Cohen, M. L. Delitsky, J. C. Pearson, and H. S. P. Muller, J. Quant. Spectrosc. Rad. Transfer **60**, 883-890 (1998).

[25]L. White and B. Boashash, IEEE Trans. Acoust., Speech, and Signal Processing **36**, 417-420 (1988).

[26]R. Latif, E. H. Aassif, G. Maze, A. Moudden, and B. Faiz, NDT E Int. **32**, 415-422 (1999).

[27]A. Vint, G. Burt, and R. Letizia, IEEE Trans. Plasma Sci. **48**, 1202 (2020).